Structural, electronic and optical properties of gold nitrides

Mohammed S H Suleiman[1,2] and Daniel P Joubert[1]

School of Physics, University of the Witwatersrand, Johannesburg, South Africa
Department of Physics, Sudan University of Science and Technology, Khartoum, Sudan

E-mail: `suleiman@aims.ac.za (M Suleiman)`

Abstract. The atomic and electronic structures of AuN, AuN_2 and Au_3N are investigated using first-principles density-functional theory (DFT). We studied cohesive energy vs. volume data for a wide range of possible structures of these nitrides. Obtained data was fitted to Birch-Murnaghan third-order equation of state (EOS) so as to identify the most likely candidates for the true crystal structure in this subset of the infinite parameter space, and to determine their equilibrium structural parameters. The analysis of the electronic properties was achieved by the calculations of the band structure and the total and partial density of states (DOS). Some possible pressure-induced structural and electronic phase transitions have been pointed out. Further, we performed G_0W_0 calculations within the the random-phase approximation (RPA) to the dielectric tensor to investigate the optical spectra. Obtained results were compared with theory and with experiment.

1. Introduction

In 2002, Šiller and co-workers [1] reported direct observation of the formation the of Au_xN compound for the first time. Since then, single crystal and polycrystalline gold nitrides have been prepared with different methods [2, 3], and many theoretical [4, 5, 6, 7] and experimental [4, 8, 2, 9, 10] investigations on the structural and physical properties of gold nitride have been published. It turned out that gold nitride possesses interesting properties which may lead to potential practical applications [11].

So far, the most significant finding may be that of Šiller et. al [8] who, in 2005, reported the production of metallic large area gold nitride films which are $\sim 50\%$ harder than pure gold films produced under similar conditions, making the gold nitride ideal for use in large-scale applications in coatings and in electronics. Moreover, the possibility of patterning gold nitride film surfaces by electron/photon beam lithography was confirmed [11].

From their experimental observations and *ab initio* calculations, Krishnamurthy *et al.* [4] suggested the possiblity of formation of more than one gold nitride phase. Although theoretical calculations have predicted several possible structures for AuN, AuN_2 and Au_3N, none of these agrees with experiment [2]. In the current first-principles study, we consider AuN, AuN_2 and Au_3N formulas in possible crystal structures. AuN is investigated in the following nine structures: NaCl (B1) structure, CsCl (B2) structure, the hexagonal structure of BN (B_k), the hexagonal structure of WC (B_h), wurtzite structure (B4), cooperite structure (B17), and the face-centered orthorhombic structure of TlF (B24). AuN_2 was investigated in the following four structures: fluorite structure (C1), pyrite structure (C2), marcasite structure (C18), and

the simple monoclinc structure of $CoSb_2$. While for Au_3N, the following five structures were considered: the fcc structure of $AlFe_3$ ($D0_3$), the simple cubic structure of Cr_3Si (A15), the anti-ReO_3 structure ($D0_9$), and the sc structure of Cu_3Au ($L1_2$).

2. Calculation methods

Our electronic structure calculations were based on spin density functional theory (SDFT) [12, 13] within the projector augmented wave (PAW) method [14, 15] in which scalar kinematic relativistic effects are incorporated via mass-velocity and Darwin corrections in the construction of the pseudo-potentials, as implemented in VASP package [16, 17]. In solving Kohn-Sham (KS) equations [18]

$$\left\{ -\frac{\hbar^2}{2m_e}\nabla^2 + \int d\mathbf{r}' \frac{n(\mathbf{r}')}{|\mathbf{r}-\mathbf{r}'|} + V_{ext}(\mathbf{r}) + V_{XC}^{\sigma,\mathbf{k}}[n(\mathbf{r})] \right\} \psi_i^{\sigma,\mathbf{k}}(\mathbf{r}) = \epsilon_i^{\sigma,\mathbf{k}} \psi_i^{\sigma,\mathbf{k}}(\mathbf{r}), \tag{1}$$

the pseudo part of the KS one-electron spin orbitals $\psi_i^{\sigma,\mathbf{k}}(\mathbf{r})$ are expanded on a basis set of plane-waves (PWs) with energy cut-off $E_{cut} = 600$ eV. $\mathbf{\Gamma}$-centered Monkhorst-Pack meshes [19] were used to sample the first Brillouin zone (BZ), and the Perdew-Burke-Ernzerhof (PBE) parametrization [20] of the generalized gradient approximation (GGA) [21] was used for the exchange-correlation (XC) potentials. For static calculations of the total electronic energy and the density of state (DOS), partial occupancies were set using the tetrahedron method with Blöchl corrections, while in the geometry relaxation, the smearing method of Methfessel-Paxton (MP) was followed.

To study the energy-volume $E(V)$ equation of state (EOS), and to determine the equilibrium parameters of each structure, we make isotropic variations of the cell volume while ions with free internal parameters were allowed to search for local minima on the Born-Oppenheimer potential hyper-surface [22], following the implemented conjugate-gradient (CG) algorithm, untill all Hellmann-Feynman force components [23] on each ion were smaller than $1 \times 10^{-2} eV/\mathring{A}$. The obtained cohesive energies E_{coh}, as a function of volume V per atom, were fitted to a Birch-Murnaghan 3rd-order equation of state (EOS) [24], and the equilibrium volume V_0, the equilibrium cohesive energy E_0, the equilibrium bulk modulus B_0 and its pressure derivative B_0' were determined by a least-squares method.

In order to improve the calculated electronic structure, and to investigate the optical spectra, we carried out G_0W_0 calculations [25, 26] within the random-phase approximation (RPA) to the dielectric tensor. From the real $\varepsilon_{re}(\omega)$ and the imaginary $\varepsilon_{im}(\omega)$ parts of this frequency-dependent microscopic dielectric tensor we derive the frequency-dependent absorption coefficient $\alpha(\omega)$, reflectivity $R(\omega)$, refractive index $n(\omega)$, and energy-loss spectrum $L(\omega)$.

3. Results and discussions

3.1. Equation of states and structural properties

In Fig. (1), $E_{coh}(V)$ curves are displayed. It is clear that the simple tetragonal structure of cooperite (B17) would be the energetically most stable structure of AuN (Fig. 1(a)). This structure was theoretically predicted to be the ground-state structure of PtN [27], and we found it to be the most stable structure of CuN as well [28]. Kanoun and Said [6] studied the $E(V)$ EOS for AuN in the B1, B2, B3 and B4 structures. Within this parameter sub-space, the relative stabilities they arrived at agree in general with ours, however Fig. 1(a) shows that B4 is prefered against B3 and only at low pressures, while they predicted that B3 is always more stable than B4.

In the AuN_2 series, the least symmetric simple $CoSb_2$ monoclinc structure is found to be the most stable (Fig. 1(b)). This agrees with the conclusion of Ref. [7] where it is suggested that

AuN_2 may be synthesized at extreme conditions (higher pressure and temperature) and/or it may have other Au:N stoichiometric ratios.

Fig. 1(c) shows that $D0_9$ is the most stable in the studied Au_3N series. $D0_9$ structure is known to be the structure of the synthesized Cu_3N. Krishnamurthy *et al.* [4] studied all these Au_3N structures and found $D0_9$ to be the most stable. Yet, they identified a triclinic crystal structure with 1.0 eV per Au_3N unit below that of $D0_9$.

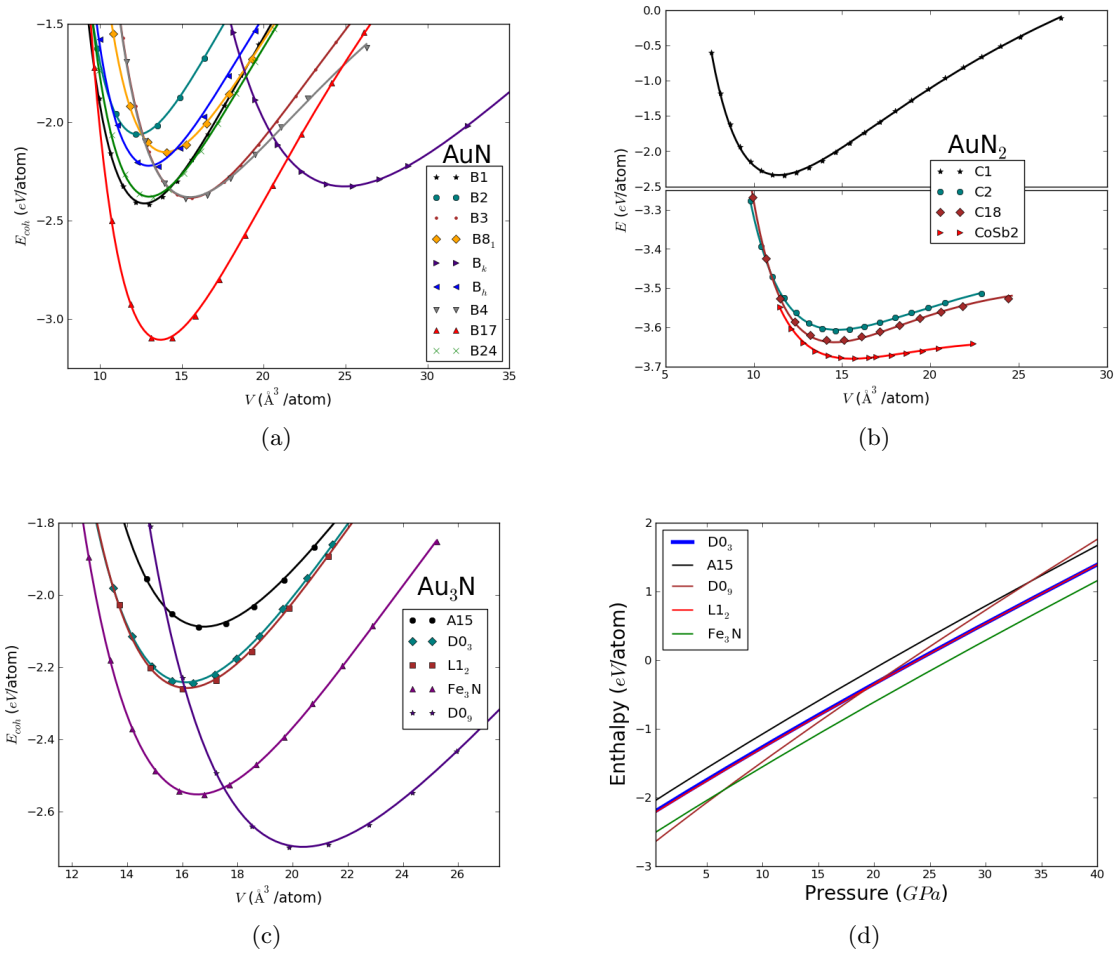

Figure 1: (Color online.) Cohesive energy $E_{\rm coh}(eV/\text{atom})$ versus atomic volume V (Å^3/atom) for (a) AuN in nine different structural phases, (b) for AuN_2 in four different structural phases, (c) for Au_3N in five different structural phases; (d) and enthalpy versus pressure for Au_3N in the five structures.

In table 1, we present some of our obtained equilibrium structural parameters and compare them with some previous theoretical calculations.

3.2. Pressure-induced phase transitions

Enthalpy-pressure relations for Au_3N in the considered structures are displayed in Fig. (1(d)). A point at which enthalpies $H = E_{coh}(V) + PV$ of two structures are equal defines the transition

Table 1. Calculated zero-pressure structural properties of some of the studied phases of AuN, AuN_2 and Au_3N**:** Lattice constants ($a(\mathring{A})$, $b(\mathring{A})$, $c(\mathring{A})$ and $\beta(^\circ)$), equilibrium atomic volume $V_0(\mathring{A}^3/\text{atom})$, cohesive energy $E_{\text{coh}}(eV/\text{atom})$, bulk modulus B_0 (GPa) and its pressure derivative B_0'. The cited data are of previous DFT calculations.

Phase	a(Å)	b(Å)	c(Å)	$\beta(^\circ)$	V_0 (Å^3/atom)	$E_{\text{coh}}(eV/\text{atom})$	B_0 (GPa)	B_0'
AuN(B17)	3.149	–	5.543	–	13.74	-3.115	176.8	5.3
$AuN_2(CoSb_2)$	6.011	5.869	10.656	151.2	15.64	-3.679	12.0	9.0
	8.149 [7]	5.350 [7]	5.361 [7]	131.09 [7]	14.68 [7]	–	–	–
AuN_2(C18)	5.162	–	–	–	11.46	-2.346	195.1	4.9
	5.144 [5]	–	–	–	15.11 [7]	–	198 [5]	
$Au_3N(D0_9)$	4.335	–	–	–	20.38	-2.702	95.4	5.5
	4.239 [4]	–	–	–	–	–	–	–

pressure P_t, where transition from the phase with higher enthalpy to the phase with lower enthalpy may occur.

Fig. (1(d)) shows that a transition from $D0_9$ phase to the Fe_3N phase would take place at a very low pressure $\sim$ 6.3 GPa; and it is clear that the $D0_9$ phase is favourable only at low pressures below $\sim$ 6.3 GPa, while the Fe_3N hexagonal structure of Ni_3N is favoured at higher pressures . Fig. (1(d)) also reveals that $L1_2$ and $D0_3$ phases may co-exist over a wide range of pressure and that they are both favoured over $D0_9$ phase at pressures higher than $\sim$ 20 GPa, while A15 would be favoured over $D0_9$ only at pressures higher than $\sim$ 33 GPa.

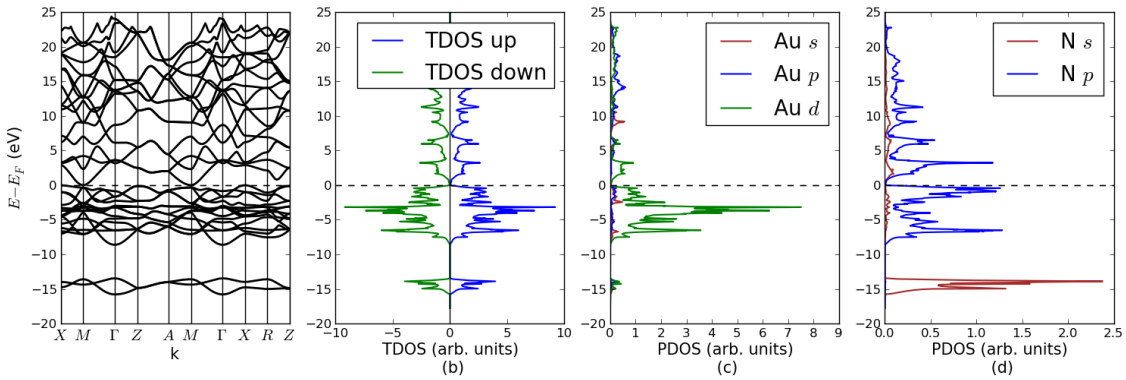

Figure 2: (Color online.) DFT calculated electronic structure for AuN in the B17 structure: **(a)** electronic band structure along the high-symmetry **k**-points. The coordinates of the labeled points w.r.t. the reciprocal lattice primitive vectors are: $X(0.0, 0.5, 0.0)$, $M(0.5, 0.5, 0.0)$, $\Gamma(0.0, 0.0, 0.0)$, $Z(0.0, 0.0, 0.5)$, $A(0.5, 0.5, 0.5)$ and $R(0.0, 0.5, 0.5)$; **(b)** spin-projected total density of states (TDOS); **(c)** partial density of states (PDOS) of Au(s, p, d) orbitals in AuN; and **(d)** PDOS of N(s, p) orbitals in AuN.

3.3. Electronic properties

The DFT(GGA) calculated electronic band structures for AuN(B17) and $Au_3N(D0_9)$ and their correponding total and partial DOS are displayed in Fig. 2 and Fig. 3, respectively. Although it might not be clear on the graph, AuN(B17) shows a very small 0.013 eV $(X - M)$ indirect DFT band gap. Krishnamurthy *et al.* [4] predicted $Au_3N(D0_9)$ to be an indirect band-gap

semiconductor, but they did not give a value. Fig. 3 shows that it is indeed a semiconductor with an $(R-X)$ indirect DFT band gap of 0.139 eV GGA value. According to the fact that the produced gold nitrides are metallic, the $D0_9$ structure may not be the true candidate for the most likely stoichiometry, Au_3N.

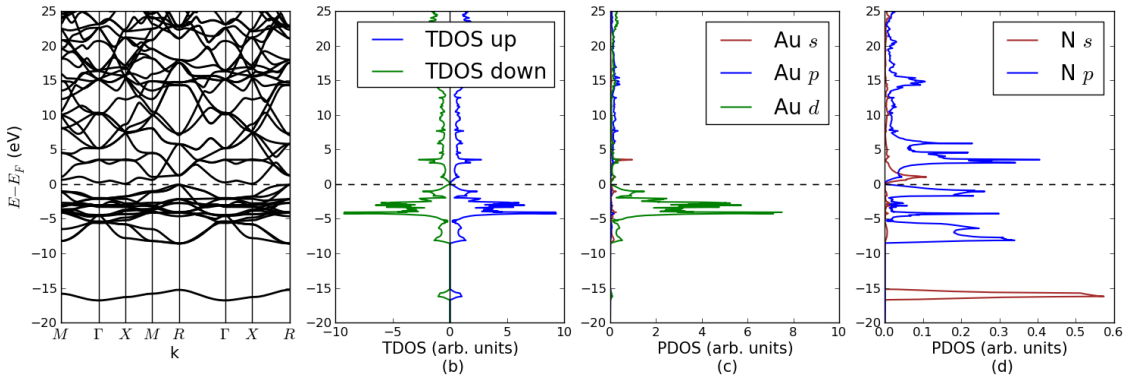

Figure 3: (Color online.) DFT calculated electronic structure for Au_3N in the $D0_9$ structure: **(a)** electronic band structure along the high-symmetry **k**-points. The coordinates of the labeled points w.r.t. the reciprocal lattice basis vectors are: $M(0.5, 0.5, 0.0)$, $\Gamma(0.0, 0.0, 0.0)$, $X(0.0, 0.5, 0.0)$ and $R(0.5, 0.5, 0.5)$; **(b)** spin-projected total density of states (TDOS); **(c)** partial density of states (PDOS) of $Au(s, p, d)$ orbitals in Au_3N; and **(d)** PDOS of $N(s, p)$ orbitals in Au_3N.

3.4. Optical properties

Fig. 4 displays the real and the imaginary parts of the frequency-dependent dielectric function $\varepsilon_{\mathrm{RPA}}(\omega)$ of $Au_3N(D0_9)$ and the corresponding derived optical constants within the visible spectrum. It is clear from the absorption coefficient $\alpha(\omega)$ spectrum that G_0W_0 calculations give a band gap of $\sim 1\ eV$, which is a significant correction to the obtained DFT value.

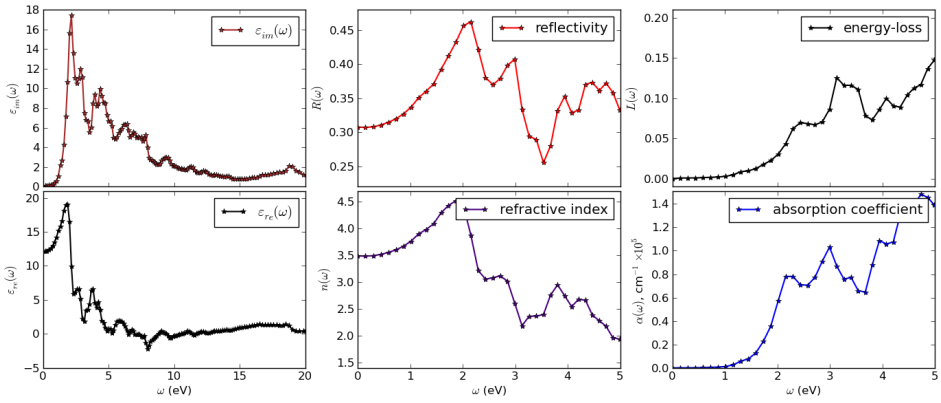

Figure 4: (Color online.) The real and the imaginary parts of the frequency-dependent dielectric function of and the corresponding optical constants of $Au_3N(D0_9)$.

4. Summary

We have applied first-principles methods to investigate the structural, electronic and optical properties of some possible stoichiometries and crystal structures of gold nitrides. The metallic B17, $CoSb_2$ and the semiconducting $D0_9$ phases have been found to be the energetically most stable structures in the studied AuN, AuN_2 and Au_3N series, respectively. The GW calculated optical spectra confirmed the semiconducting nature of $D0_9(Au_3N)$ and corrected the DFT calculated band gap. Obtained results show good agreement with previous studies.

Acknowledgments

Suleiman would like to thank Dr. Mahlaga P. Molepo for his valuable discussions and support. Many thanks to Mr. Ross McIntosh for his comments.

References

[1] Šiller L, Hunt M, Brown J, Coquel J M and Rudolf P 2002 *Surface Science* **513** 78 – 82 ISSN 0039-6028
[2] Alves L, Hase T P A, Hunt M R C, Brieva A C and Šiller L 2008 *Journal of Applied Physics* **104** 113527 (pages 5)
[3] Šiller L, Alves L, Brieva A, Butenko Y and Hunt M 2009 *Topics in Catalysis* **52**(11) 1604–1610 ISSN 1022-5528 10.1007/s11244-009-9281-6
[4] Krishnamurthy S, Montalti M, Wardle M G, Shaw M J, Briddon P R, Svensson K, Hunt M R C and Šiller L 2004 *Physical Review B* **70**(4) 045414
[5] Yu R and Zhang X F 2005 *Physical Review B* **72**(5) 054103
[6] Kanoun M and Goumri-Said S 2007 *Physics Letters A* **362** 73 – 83 ISSN 0375-9601
[7] Chen W, Tse J and Jiang J 2010 *Solid State Communications* **150** 181 – 186 ISSN 0038-1098
[8] Šiller L, Peltekis N, Krishnamurthy S, Chao Y, Bull S J and Hunt M R C 2005 *Applied Physics Letters* **86** 221912 (pages 3)
[9] Quintero J H, Ospina R, Crdenas O O, Alzate G I and Devia A 2008 *Physica Scripta* **2008** 014013
[10] Brieva A C, Alves L, Krishnamurthy S and Siller L 2009 *Journal of Applied Physics* **105** 054302 (pages 4)
[11] Butenko Y, Alves L, Brieva A, Yang J, Krishnamurthy S and Šiller L 2006 *Chemical Physics Letters* **430** 89 – 92 ISSN 0009-2614
[12] von Barth U and Hedin L 1972 *Journal of Physics C: Solid State Physics* **5** 1629–1642
[13] Pant M and Rajagopal A 1972 *Solid State Communications* **10** 1157 – 1160 ISSN 0038-1098
[14] Blöchl P E 1994 *Physical Review B* **50**(24) 17953–17979
[15] Kresse G and Joubert D P 1999 *Physical Review B* **59**(3) 1758–1775
[16] Kresse G and Hafner J 1993 *Physical Review B* **47**(1) 558–561
[17] Kresse G and Hafner J 1994 *Physical Review B* **49**(20) 14251–14269
[18] Kohn W and Sham L J 1965 *Physical Review* **140**(4A) A1133–A1138
[19] Monkhorst H J and Pack J D 1976 *Physical Review B* **13**(12) 5188–5192
[20] Perdew J P, Burke K and Ernzerhof M 1996 *Physical Review Letters* **77**(18) 3865–3868
[21] Becke A D 1988 *Physical Review A* **38**(6) 3098–3100
[22] Born M and Oppenheimer J R 1927 *Annalen der Physik* **84** 457–484
[23] Feynman R P 1939 *Physical Review* **56**(4) 340–343
[24] Birch F 1947 *Physical Review* **71**(11) 809–824
[25] Hedin L 1965 *Physical Review* **139**(3A) A796–A823
[26] Shishkin M and Kresse G 2006 *Physical Review B* **74**(3) 035101
[27] von Appen J, Lumey M W and Dronskowski R 2006 *Angewandte Chemie International Edition* **45** 4365–4368 ISSN 1521-3773
[28] Suleiman M S H, Molepo M P and Joubert D P 2012 *ArXiv e-prints* (*Preprint* 1211.0179)